Interfacial processes studied by coupling electrochemistry at the polarised liquid-liquid interface with in situ confocal Raman spectroscopy

Lukasz Poltorak, M. Dossot, Grégoire Herzog, Alain Walcarius

Interfacial processes studied by coupling electrochemistry at the polarised liquid-liquid interface with *in-situ* confocal Raman spectroscopy

Lukasz Poltorak, Manuel Dossot, Grégoire Herzog,* Alain Walcarius

Laboratoire de Chimie Physique et Microbiologie pour l'Environnement (LCPME), UMR 7564, CNRS – Université de Lorraine, 405 rue de Vandœuvre, 54600 Villers-lès-Nancy, France.

*Corresponding author: gregoire.herzog@univ-lorraine.fr

This document is a post-print. Final version has been published in *Physical Chemistry Chemical Physics* 16 (2014) 26955-26962 (https://doi.org/10.1039/C4CP03254C).

Abstract

Interfacial processes controlled by ion transfer voltammetry at the interface between two immiscible electrolyte solutions were studied by in-situ Raman spectroscopy. Raman spectra of the interface between a 5 mM NaCl aqueous solution and a 10 mM bis(triphenyl-phosphoranydieneammonium) tetrakis(4-chlorophenyl)borate in 1,2-dichloroethane were recorded at open circuit potential and at various interfacial potential differences. At open-circuit potential, Raman peaks assigned to vibrational modes of 1,2-dichloroethane are clearly visible and peaks of weak intensity are measured for the organic electrolyte ions. When a negative interfacial potential difference is applied, the intensity of the peaks of the cation of the organic electrolyte increases, confirming its transfer induced by the interfacial potential difference applied. The electrochemically assisted generation of mesoporous silica deposits was then followed by *in-situ* confocal Raman spectroscopy. The condensation of mesoporous silica was controlled by the transfer of cetyltrimethylammonium (CTA^+) ions to an aqueous

phase containing hydrolysed silanes. The transfer of CTA^+ at the interface was monitored *in-situ* by confocal Raman spectroscopy, and formation of silica was observed.

Introduction

An interface between two immiscible electrolyte solutions (ITIES) is formed between two liquid solvents of a low (ideally zero) mutual miscibility, each containing an electrolyte.[1] Usually, one of these is a water solution of hydrophilic electrolyte, whereas the latter is a polar organic solvent allowing dissociation of hydrophobic electrolyte. Electrochemistry at the ITIES allows a number of applications: the study of ion-transfer across the phospholipid monolayers modified ITIES,[2] electroanalysis not restricted to electron transfer (oxidation and reduction) reactions,[3,4] or ion extraction in hydrodynamic conditions,[5] for instance. The ITIES is defect-free and self-healing - down to the molecular scale[6] – and these properties are employed for the electrodeposition of free standing metal films,[7,8,9,10] metal-organic polymer composites[11] or inorganic polymer framework of silica material.[12,13,14] This last category is particularly important as mesoporous materials are of paramount interest for electrode modification.[15] For example, the electrochemically controlled sol-gel process using a surfactant template allows the synthesis of silica materials of highly ordered structure and vertically-aligned pore channels.[16] Such template-directed porous electrodes are very attractive in electroanalysis and for the development of electrochemical sensors.[17] In our previous works, we have demonstrated the electrogeneration of porous silica deposits at the ITIES, at both macroscopic and microscopic ITIES.[13,14] The process is controlled by ion transfer voltammetry of the surfactant template from the organic phase to the aqueous medium containing the silica precursors. The films obtained exhibit low-distance type of symmetry with pores having worm-like structure, with the average pore centre-to-centre distance changing upon different experimental conditions.[13] Morphological study conducted by scanning electron microscopy and shear-force profilometry has shown that silica deposits always grow on the aqueous side of interface. This is due to the transfer of surfactant ions from the organic phase to the aqueous phase. Their presence at a sufficiently high

concentration favours the condensation of the hydrolysed silica precursors. The silica condensation is controlled by the diffusion of CTA^+ in the aqueous phase and the deposits tend to form hemispheres at longer deposition times.[14]

In general, electrochemistry at the ITIES allows the estimation of thermodynamic, kinetic, adsorption and charge transfer parameters, but precise quantitative information about the interfacial region has to be supported by other methods. Spectroscopic methods (both linear and non-linear techniques) can be coupled to electrochemistry at the ITIES.[18] The greatest challenge lies with the separation of the signal originating from the bulk from the signal originating from the interfacial region. This can be overcome by fulfilling the condition of total internal reflection.[18] The first studies of interfacial processes by spectroelectrochemistry were made using linear techniques, which include UV-visible volt- and chronoabsorptometry[19,20,21], volt- and chronofluorometry[22,23] or reflectance spectroscopy.[24] On the contrary, non-linear techniques (sum frequency spectroscopy and second harmonic generation) have provided information about the molecular structure of liquid/liquid interface as they are surface specific.[25] Confocal Raman spectroscopy can also be used to focus the analysis at the interface and provide useful interfacial information. Raman spectroscopy with a spatial resolution 0.5 – 1μm has been used to investigate electron transfer reaction at microelectrode arrays.[26,27] Raman spectroscopy has also often been used for the characterisation of reactions occurring at the interface between two immiscible phases.[28–35] Interfacial reactions[28] or metallic nanoparticles self-assembly[29–33] at the liquid-liquid interface were monitored by Raman spectroscopy. However, the investigation of reactions at the liquid-liquid interface controlled by electrochemical means has scarcely been studied. Indeed, it was only recently that surface enhanced Raman scattering was used to study the potential dependent agglomeration of silver nanoparticles at water/1,2-dichloroethane (DCE) interface.[33] The electrodeposition of gold nanoparticles formed at a three-phase junction was

also investigated by surface enhanced Raman spectroscopy.[36] The association of electrochemistry and Raman techniques at microscopic liquid-liquid interfaces allows the collection of complementary data on the mechanism involved in the electrochemically-assisted generation of surfactant-templated silica films at such interfaces.

In the present work, an experimental set-up was developed to couple electrochemical measurements at the ITIES with Raman confocal microscopy. The incident laser was focused on both macroscopic and microscopic interfaces to allow the recording of Raman spectra at open circuit potential and upon the application of interfacial potential differences. Finally, the changes in interfacial molecular composition of μITIES were studied during the presence of silica deposit formation.

Experimental section

Chemicals and reagents

Chemicals were used as received: Bis(triphenylphosphoranyldiene) ammonium chloride, ($BTPPA^+Cl^-$, 97%, Aldrich), potassium tetrakis(4-chlorophenylborate), (K^+TPBCl^-, ≥98%, Fluka), sodium chloride, (NaCl, ≥98%, Prolabo), cetyltrimethylammonium bromide (CTAB, ≥99%, Acros Organics), tetraethoxysilane (TEOS, 98%, Alfa Aesar), lithium chloride (LiCl, ≥99%, Aldrich), ferric chloride hexahydrate ($FeCl_3 \cdot 6H_2O$, 99 – 102%, Fluka), HCl (1M, volumetric solution, Riedel-de Haen), NaOH (pellets, pure, Riedel-de Haen), and 1.2-dichloroethane (DCE, ≥99%, Sigma-Aldrich). $BTPPA^+TPBCl^-$ (organic electrolyte) and CTA^+TPBCl^- (template salt) were prepared via simple metathesis reaction between $BTPPA^+Cl^-$ and K^+TPBCl^- and CTAB and K^+TPBCl^- respectively (procedure of preparation reported elsewhere).[13] NaCl and LiCl were used as aqueous electrolytes whereas TEOS was used as silica precursor. Solution pH was tuned with HCl (1M) and NaOH (1M) to allow hydrolysis (pH = 3) and condensation (pH = 9.5) of TEOS. The high density organic phase

was a 1,2-dichloroethane (DCE) whereas the low density phase was high purity H_2O obtained from a water purification system (I + quality, Purelab, Elga).

Coupled electrochemical – spectroscopic set-up

Experiments were carried out at both macroscopic and microscopic interfaces. Raman spectra at open-circuit potential were recorded at macroscopic interfaces, for which a classical liquid-liquid electrochemical cell was used.[1] All the Raman spectra recorded upon the application of the interfacial potential difference were obtained at an array of micro-interfaces, which were supported by a silicon wafer pierced with regularly aligned holes. The fabrication procedure for the micro-interface array (μITIES) was reported elsewhere.[37] The *in-situ* confocal Raman spectroscopy study of electrochemical silica material formation at the μITIES was performed in the custom-made cell presented in Figure 1a. A water immersion objective with long working distance and X60 magnification (focal length: 7 mm), as well as the platinum mesh electrode (aqueous counter electrode) and Ag/AgCl electrode (aqueous reference electrode) were immersed into aqueous phase filling the PTFE vessel. The silicon wafer supporting the array of μITIES (shown in Figure 1b) was fixed to a glass capillary with silicone acetate sealant (resistant to DCE). The capillary was placed into the aqueous phase through the hole at the bottom of the cell. In order to prevent aqueous phase leakage the gasket was employed. The μITIES membrane design involves three parameters, namely: membrane thickness (d = 100μm), pore center-to-center distance (S = 100 μm) and pore radius (r = 10 μm). Fig. 1c represents composition of aqueous phase: hydrolysed TEOS being the silica deposit precursor and NaCl constituting aqueous phase electrolyte. In turn, Figure 1d, shows the species dissolved in organic phase, which are $BTPPA^+TPBCl^-$ (organic electrolyte) and CTA^+TPBCl^- (template salt).

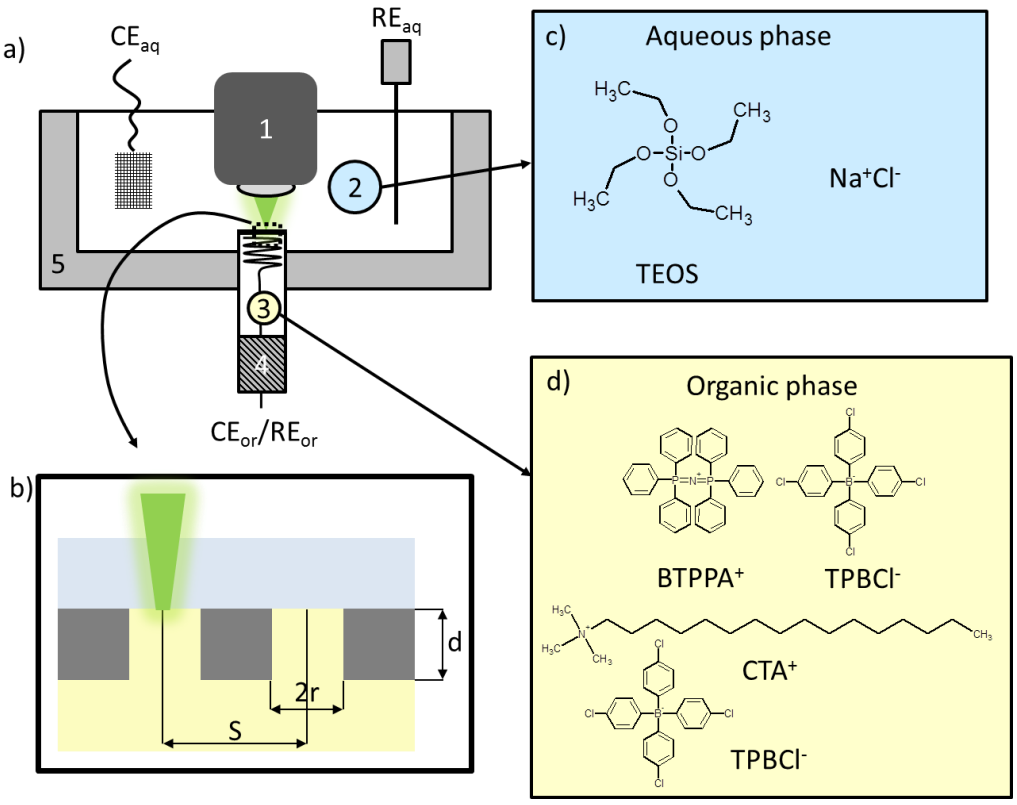

Figure 1. a) The custom-made electrochemical cell was used in *in-situ* confocal Raman spectroscopy study of electrochemical silica material formation at the µITIES. The objective (1) was placed directly in the aqueous phase (2) filling the PTFE vessel (5). The organic phase (3) was placed inside the capillary. The stopper (4) was made from silicon rubber. A detailed view of the silicon wafer supporting array of pores is shown in part b). The hydrophobic character of the pore walls ensures the presence of organic phase inside the pores during the experiment. Part c) and d) represents composition of aqueous and organic phase respectively. Designations: CE_{aq} – aqueous counter electrode, RE_{aq} – reference aqueous electrode, CE_{or}/RE_{or} – counter and reference organic electrode, *S* – pore center-to-center distance (100 µm), *r* – pore radius (10 µm) and *d* – membrane thickness (100 µm).

The electrochemical cell was Ag | AgCl | x mM hydrolysed TEOS + 5 mM NaCl (aqueous) ‖ y mM CTA^+ $TPBCl^-$ in 10 mM $BTPPA^+$ $TPBCl^-$ (DCE) | 10 mM LiCl + 10 mM $BTPPA^+$ Cl^- (saturated) (aqueous) | AgCl | Ag. The interfacial potential difference was controlled using a PGSTAT 302N (Autolab, Metrohm, Switzerland). Confocal Raman spectroscopy measurements were carried out with a Horiba Jobin Yvon T64000 spectrometer with a green light laser and equipped with a nitrogen cooled CCD detector. The laser wavelength was

either 532 or 514 nm. The spectra recorded at these wavelength were fully consistent at both wavelengths as no electronic resonance was observed. The irradiance was measured in air at 100 kW cm^{-2}. We estimated that the irradiance in the aqueous phase is around the same value. No laser heating effect was observed as the aqueous phase volume was large enough to ensure heat dissipation. Unless stated otherwise, the Raman spectrum peaks were assigned based on the Handbook of Infrared and Raman Characteristic Frequencies of Organic Molecules.[38]

Results and discussion

Electrochemically assisted generation of silica at the liquid-liquid interface

The liquid-liquid interface was prepared with an organic electrolyte solution, which contains a surfactant (i.e., CTA^+) acting as both a condensation catalyst and a template, and an aqueous electrolyte solution, which contains the hydrolysed form of the silica precursors (TEOS). Spontaneous formation of silica deposit was not observed and ion transfer voltammetry was needed to condensate the silica.[13] A typical cyclic voltammogram for the formation of silica deposit at µITIES is shown in Figure 2. The sharp negative current increase appearing between +0.1 and 0.0 V was due to the transfer of CTA^+ ions from the organic phase to the aqueous one. This transfer was possible only in the presence of silica precursors in the aqueous phase, suggesting some type of assisted ion transfer.[13] The polarization direction – from more to less positive potential range – was in agreement with the positive charge of template molecules, which are transferred from the organic to the aqueous phase. Once being transferred to the aqueous phase, CTA^+ ions form charged micelles, around which the silica species are condensed. On the reverse scan, the peak for partial CTA^+ back transfer was observed at +0.24 V. Silica deposition involved encapsulation of template species and hence the CTA^+ transfer was not reversible. Further change in polarization results only in capacitive

current. Scheme 1 illustrates the mechanism of the silica condensation at the liquid-liquid interface, which has been discussed in detail in our previous works.[13,14]

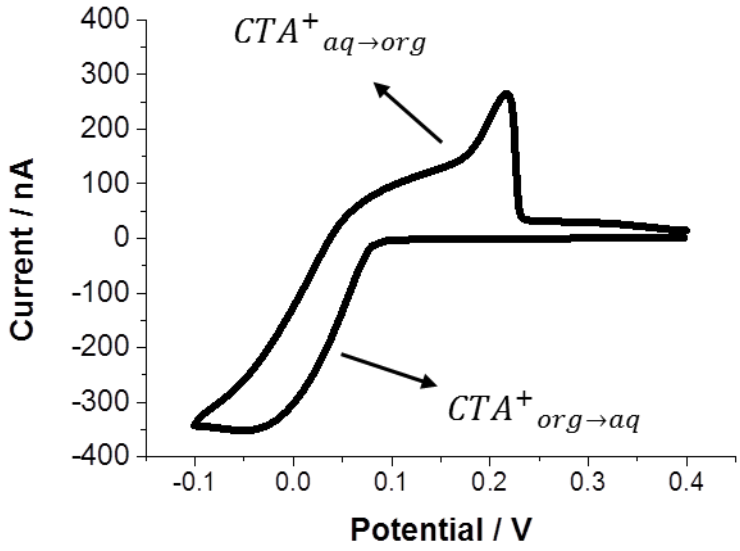

Figure 2. Cyclic voltammogram recorded at array of µITIES (r = 10 µm, S = 100 µm and N = 120) during surfactant-templated silica deposits formation. Scan rate = 5 mV s^{-1}.

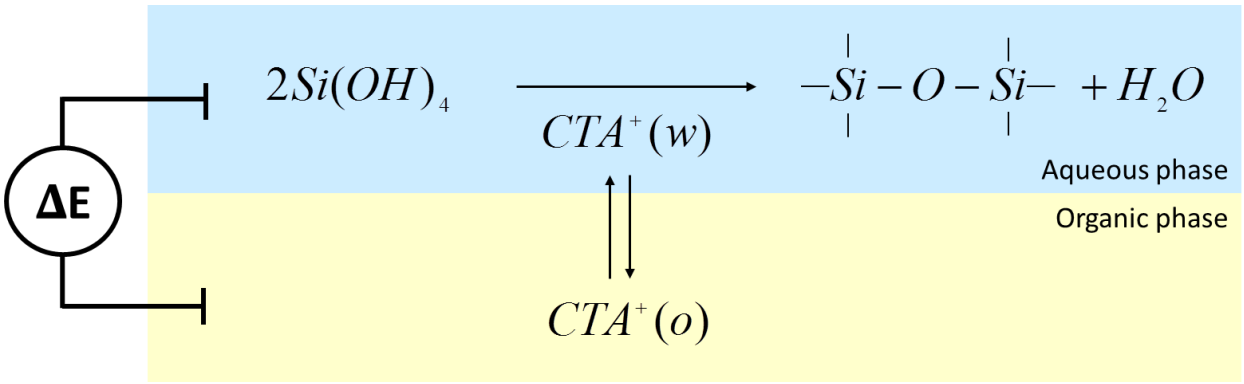

Scheme 1. Illustration of the silica formation mechanism

Raman spectroscopy analysis of the liquid-liquid interface at open circuit potential

Figure 3 shows the different Raman spectra recorded at the interface formed between a NaCl aqueous solution and DCE in the absence (Figure 3a) and in the presence of 10 mM $BTPPA^+TPBCl^-$ (Figure 3b), of 10 mM $BTPPA^+TPBCl^-$ and 14 mM CTA^+TPBCl^- (Figure 3c) and 53 mM CTA^+TPBCl^- (Figure 3d) in the organic phase. Prior to spectrum collection, the

laser was focused on the macroscopic liquid/liquid interface. Spectrum a) from Figure 3 was recorded at the liquid/liquid interface with pure DCE as the organic phase. The series of peaks obtained correspond to the peaks obtained for the Raman spectrum of pure DCE recorded in solution in the macroscopic cell (Figure SI1 of the Supplementary Information (SI) section). The peaks at 653 and 673 cm^{-1} can be assigned to the C-Cl stretching modes of the *gauche* conformer, whereas the peak at 753 cm^{-1} arises from the C-Cl A_g stretching mode of the *trans* conformer.[39] Additionally, the chloromethyl group gives two overlapping peaks around 3034 cm^{-1} (weak intensity) assigned to the antisymmetric CH_2 stretching mode and 2987 cm^{-1} (very strong intensity) assigned to the corresponding symmetric stretching mode.[40] When the organic electrolyte was added to the organic phase, three additional peaks were observed (inset of Figure 3) at 725, 1000 and 1078 cm^{-1}. The peak at 725 cm^{-1} was probably due to the aromatic C-Cl vibration and arose from the presence of the anion of the organic electrolyte. The origin of the peak at 1000 cm^{-1} was ascribed to the presence of the aromatic rings of $BTPPA^+$ (also found elsewhere[33]) and can be treated as a trace of the organic electrolyte. The peak at 1078 cm^{-1} can be assigned to the vibration of the aryl-Cl bond present only in $TPBCl^-$. These observations were in good agreement with the Raman spectra of the powders of the organic electrolyte $BTPPA^+TPBCl^-$ (Figure SI1b) of $BTPPA^+Cl^-$ (Figure SI1c) and of the K^+TPBCl^- (Figure SI1d) reported in SI. The intensity of both peaks at 725 and 1078 cm^{-1} increases with the concentration of CTA^+TPBCl^- in the organic phase (inset of Figure 3), confirming the correct attribution of these peaks to the vibrations related to $TPBCl^-$. The intensity of the peak at 1000 cm^{-1} attributed to $BTPPA^+$, remained constant upon the addition of 10 mM of CTA^+TPBCl^- in the organic phase and then drops for 53 mM of CTA^+TPBCl^- in the organic phase, suggesting that the attribution of a vibrational mode of $BTTPA^+$ was correct. Addition of CTA^+TPBCl^- to the organic electrolyte solution also gave rise to another peak at 349 cm^{-1}, which could be attributed to low-frequency deformation modes of CTA^+

alkyl chains.[38] These experiments demonstrated that organic electrolyte and surfactant ions remained in the organic phase at open-circuit potential.

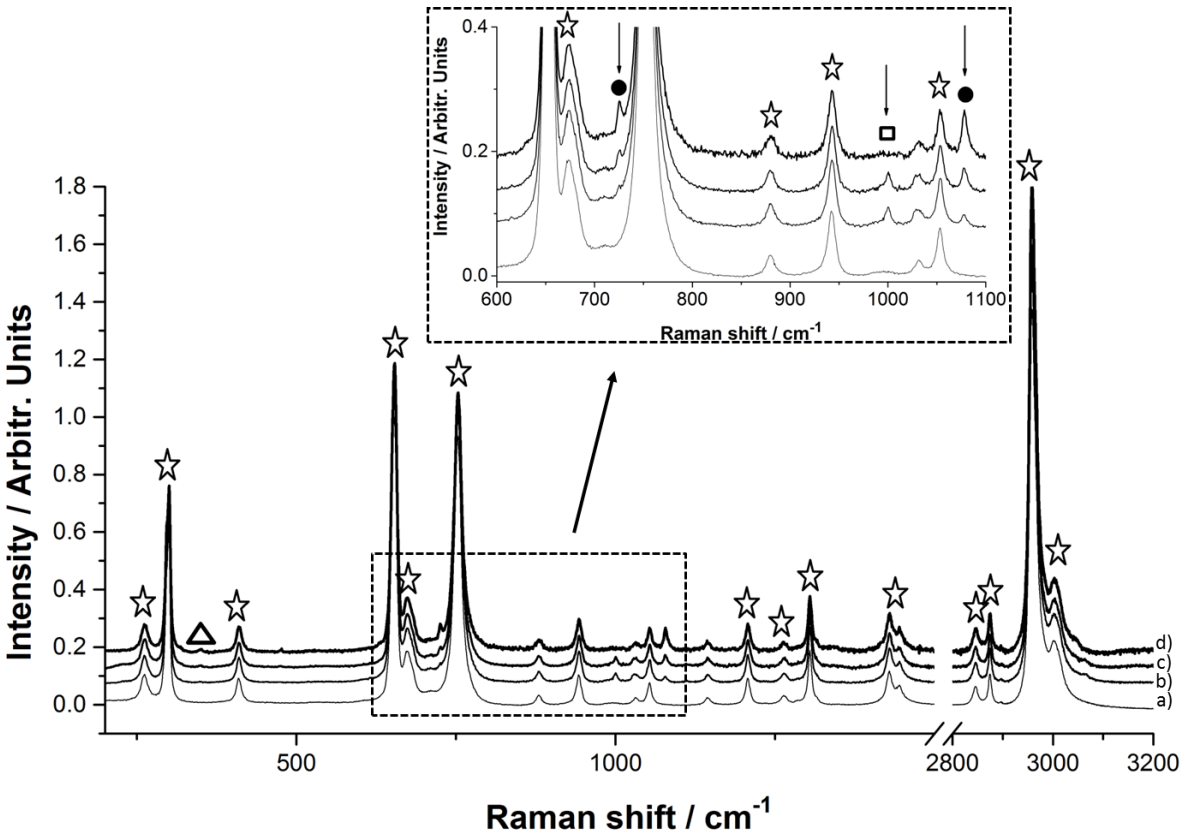

Figure 3. Raman spectra recorded at open-circuit potential at the macroscopic liquid/liquid interface constituted between 5 mM NaCl aqueous solution and: a) DCE, b) 10 mM $BTPPA^+TPBCl^-$ in DCE, c) 10 mM $BTPPA^+TPBCl^-$ and 14 mM CTA^+TPBCl^- in DCE and d) 53 mM CTA^+TPBCl^- in DCE. Raman bands marked with (□) were assigned to $BTTPA^+$, with (●) to $TPBCl^-$, with (☆) to DCE and with (**Δ**) to CTA^+.

Influence of the applied potential on Raman spectroscopy

Previous works have demonstrated that the application of a negative potential difference can cause a displacement of the interface with an ingress to the aqueous phase.[41,42] The influence of polarization potential on the position of the interface was then investigated by recording Raman spectra under various negative interfacial potential differences (see Figure 4a for the

spectral region of interest, the full spectra is given as Figure SI2 in the SI section) to ensure that variations of Raman peak intensities were due to ion transfer rather than displacement of the interface. Prior to spectrum collection, the laser spot was focused at the μITIES under open circuit potential (Figure 4a, dashed curve). Then, the interfacial potential difference was held for times sufficiently long (which was typically 4 minutes) to collect a full Raman spectrum from 200 to 3200 cm^{-1}. Spectra were normalized to the silicon peak at 520 cm^{-1} (arising from photons scattered by the silicon membrane). The interfacial potential difference was varied from -0.2 down to -0.8 V. At these potentials, $BTPPA^+$ ions are transferred from the organic phase to the aqueous phase as demonstrated on the CV shown in Figure 4c. Three types of behaviour were observed corresponding to the different molecules present in the solution.

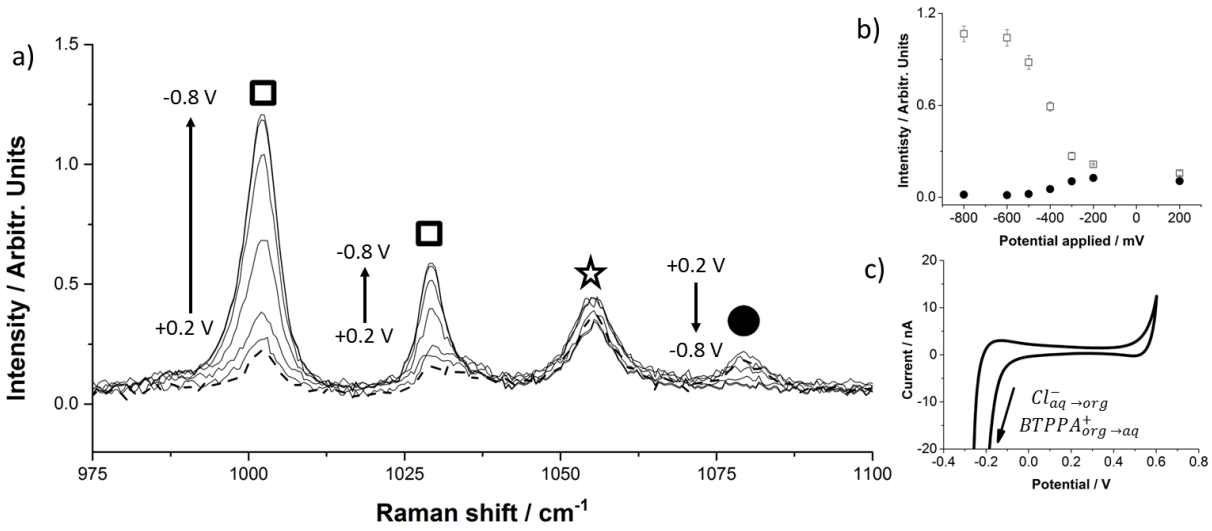

Figure 4. a) Raman spectra recorded at the μITIES between 5 mM NaCl aqueous solution and 10 mM $BTPPA^+TPBCl^-$ organic solution under different negative polarization. The insert b) shows the peak intensity (after normalization to 520 cm^{-1} band) as a function of the applied potential – (□) correspond to the peak intensities at 1002 cm^{-1} while (●) represents the peak intensities at 1078 cm^{-1} (in that case error bars are too small to notice); open circuit potential was 200 mV; Raman peaks marked with (□)

were assigned to $BTTPA^+$, with (☆) to DCE and with (●) to $TPBCl^-$. The insert c) represents the characteristic cyclic voltammogram obtained in these conditions.

As the interface was polarized at more negative potentials, all bands (653, 673, 753, 2847, 2877, 2961 and 3005 cm^{-1}) assigned to the vibrational modes of DCE decreased in intensity, which would confirm that the organic phase did not ingress to the aqueous phase (Figure SI2 in SI section). This was supported by the increase of the band intensity at 1002 and 1029 cm^{-1} related to $BTPPA^+$ ions (Figure 4b – open squares). Indeed, more and more $BTPPA^+$ ions were transferred as the interfacial potential difference became more and more negative (i.e., from -0.2 V down to -0.8 V). Furthermore, at such negative interfacial potential difference, the transfer of anions from the organic side of the interface ($TPBCl^-$) was not expected. The band intensity at 1078 cm^{-1} dropped as the interfacial potential difference varied (Figure 4b). These experiments demonstrated that ion transfer could be followed by Raman spectroscopy by Raman spectra. The variation of the peak intensity was not due to the displacement of the liquid-liquid interface.

Interfacial processes at the µITIES followed by Raman spectroscopy

The electrochemically assisted assembly of surfactant-templated silica at the µITIES was followed by Raman spectroscopy. A Raman spectrum was first recorded at open circuit potential (ocp = + 0.2 V) and it showed all the characteristic vibration bands reported in Figure 3. After this control experiment, the interfacial potential difference was linearly swept (at 5 mV s^{-1}) from +0.6 V down to -0.1 V; the potential was held at -0.1 V while a second Raman spectrum was recorded; the potential was then swept back from -0.1 V to +0.6 V where a third Raman spectrum was recorded while holding the potential at +0.6 V; the same operation was reported once more to get the 4^{th} and 5^{th} Raman spectra, which are exhibited on Figure 5a for three distinct spectral regions (Figure 5b shows the corresponding

voltammograms and potential values at which Raman spectra were recorded). After the first potential scan, interfacial properties changed and the spectrum obtained became much more complex than at open circuit potential. The arrows in the Figure 5a indicate the evolution of the particular peaks upon repetitive scans; with some of the intensities increasing with the number of scans while other drop down. The region from 2800 to 3100 cm^{-1} showed the most dramatic variations upon voltammetric cycling. This region corresponds to the C-H stretching modes, which originated from either DCE, $BTTPA^+$, $TPBCl^-$ or CTA^+ ions. The presence of CTA^+ after the first scan was confirmed by the vibrational contribution from its long alkyl chains, in particular: CH_2 symmetric stretching at 2851 cm^{-1}, CH_3 symmetric stretching at 2874 cm^{-1} and CH_3 asymmetric stretching mode at 2935 cm^{-1}. Additionally, $BTPPA^+$ and $TPBCl^-$ ions gave rise to two overlapping bands from 3025 to 3080 cm^{-1}. The band centered at 3044 cm^{-1} originated most probably from $BTPPA^+$ and arose from the five aryl C-H bonds in the aromatic rings, whereas the latter at 3064 cm^{-1} can be assigned to monosubstituted aromatic rings as in case of chlorophenyl substituent in $TPBCl^-$. The other peaks associated to $BTTPA^+$ at 1002 and 1025 cm^{-1} and to $TPBCl^-$ at 1078 and 1115 cm^{-1} also increased. If the growth of characteristic peaks assigned to CTA^+ vibration modes was expected, the increase of those related to the ions of the organic phase electrolyte was more surprising, however possible since the silica material is known to be an attractive adsorbent for coadsorption between CTA^+ and species containing aromatic rings.[43] Indeed, the spectra presented in Figure 3 had shown that these ions were barely visible at open circuit potential. Furthermore, peak intensities of the vibration modes of $BTPPA^+$ were not growing before a potential difference of -0.3 V was reached, whereas $TPBCl^-$ did not transfer at all at such negative interfacial potential difference (Figure 4). A possible explanation to such increase in the intensity of the bands characteristic to these two compounds can be trapped in the silica-surfactant matrix, which is being formed by self-assembly condensation of TEOS when CTA^+

is transferred to the aqueous phase, via favourable electrostatic interactions (i.e., between the $TPBCl^-$ anions and CTA^+ cations, and between $BTTPA^+$ cations and the negatively-charged silica surface). Such hypothesis was notably supported by previous observations made for CTA^+ – based mesoporous silica materials for which the final composition implied the presence of ionic species in addition to the presence of surfactant and silica.[44,45]

Unfortunately, no direct in situ evidence of the interfacial silica material formation was found, since no band for Si-O-Si vibrational mode had been observed during the acquisition time used in our experiments. This might be due to the fact that longer acquisition times were required to observe the Si-O-Si vibrational mode in the 450 to 500 cm^{-1} region[46] for silica films and if existing here, this signal was too weak to be visible with respect to the other ones or to the noise of the Raman spectra. Another point was that the condensation kinetics for sol-gel-derived silica is usually rather slow (i.e., low condensation degree for the material generated in the synthesis medium, as pointed out from *in situ* NMR experiments),[47,48] and required subsequent heat treatment to achieve a high degree of cross-linking of the silica network. Actually, we have been able to observe this vibration band for a silica deposit electrogenerated at the miniaturised liquid-liquid interface, but only after calcination in 450 °C for 30 minutes (see the inset in Figure 6). Long acquisition times (50 minutes to record the spectrum in whole spectral range) resulted in a broad peak in the region from 350 to 500 cm^{-1} corresponding to Si-O-Si stretching mode and small peak at 700 cm^{-1}assigned to Si-OH.

Another indirect evidence of silica formation can be seen by following the evolution of the Si-Si band at 520 cm^{-1} (see Fig. 6,). Indeed, mesoporous materials, *(e.g.* mesoporous silica) can serve as a waveguide for light.[49] The amount of the silica material generated at the µITIES grew with the number of scans, and hence disturbed the system by guiding laser photons through the silica deposit to the silicon wafer supporting the µITIES. The waveguide phenomenon (due to elastic light scattering by the silica formed) was observed as the increase

in Si-Si band intensity. The same phenomenon could be held responsible for the disappearance of all bands originating from DCE.

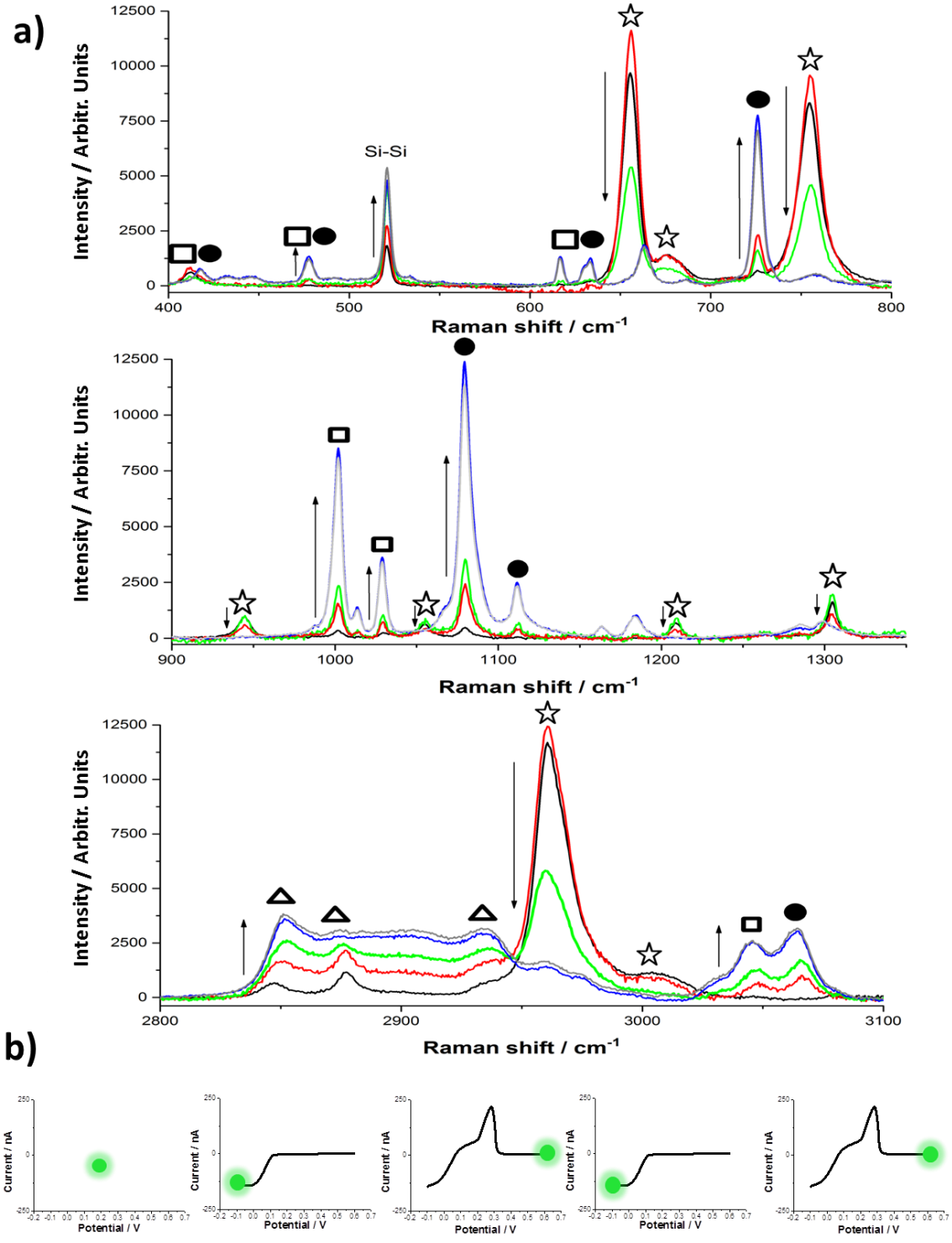

Figure 5. a) Raman spectra recorded during *in-situ* silica material formation at the μITIES in three different spectral regions. Arrows on the graphs indicate direction of peak evolution, whereas the colours correspond to the order of spectra collection (1st black, 2nd red, 3rd green, 4th blue and 5th grey).

The Raman spectrum collection was performed alternately with ion-transfer linear sweep voltammetry as it is shown schematically in part b of the graph. Raman bands marked with (□) were assigned to $BTTPA^+$, with (●) to $TPBCl^-$, with (☆) DCE and (**Δ**) to CTA^+.

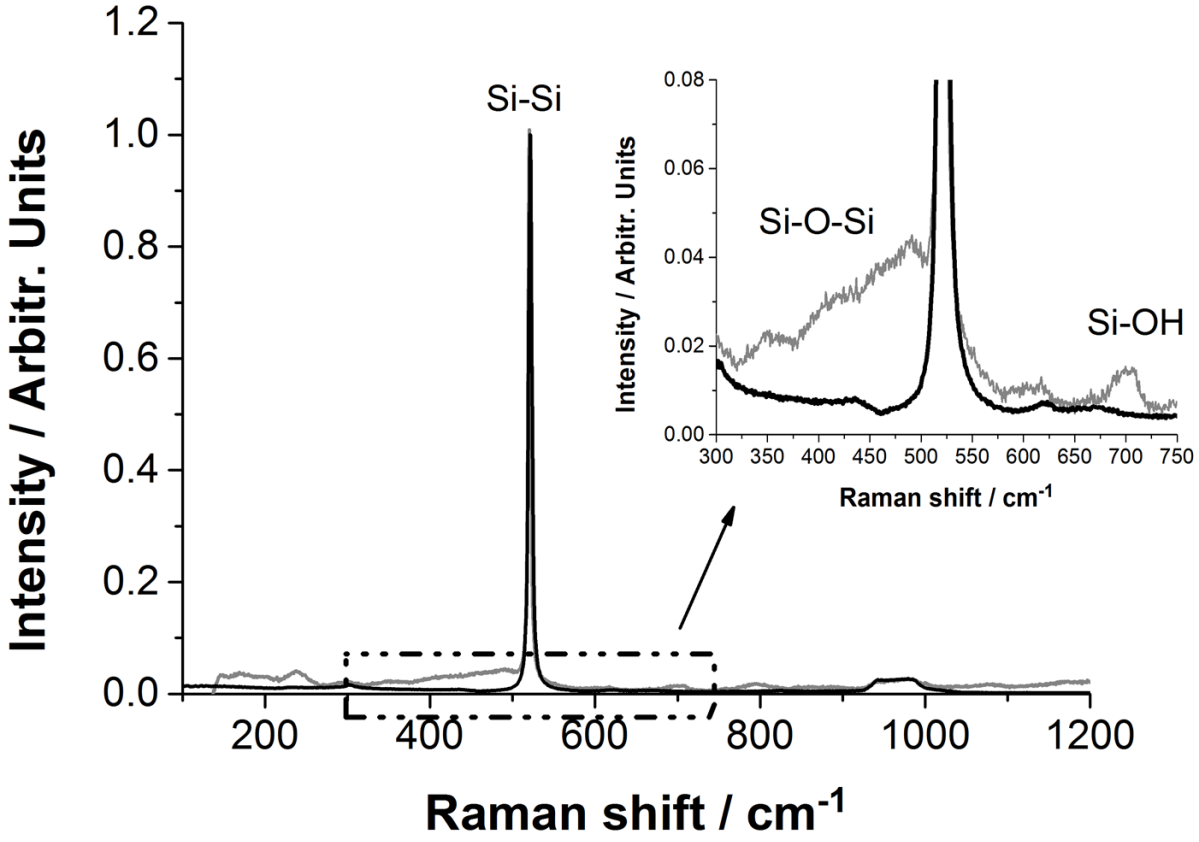

Figure 6. Raman spectra for a silicon membrane (black line) and for a silica deposit after calcination (grey line). The enlargement of the spectra in the 300 – 750 cm^{-1} region corresponds to the frequencies of vibration of silica bonds. Spectra were normalized to the Si-Si peak.

Conclusion

In this work, confocal Raman spectroscopy was used to follow interfacial processes at the polarised liquid/liquid interface. The spatial resolution (~1µm) offered by the Raman microspectrometer enabled the study of liquid-liquid interfaces in dwells of few tens of µm organized in an array format. Raman spectroscopy has been shown to be very sensitive to the change in interfacial properties induced by either ion transfer voltammetry or modification of

the interface. Ion transfer could be followed after a precise assignment of each typical vibration peak of the chemical species present in the system. The high spectral resolution of usual Raman spectrometers and the sharpness of Raman peaks were of strong help in this regard. Raman spectroscopy also offers the opportunity to monitor vibrational modes in the aqueous phase, which was more difficult in infrared absorption spectroscopy (though not impossible using dedicated techniques like ATR). The confocal microscope also enabled to finely localize the organic/aqueous phase interface, which was mandatory in this kind of study. Besides, compared to non-linear optical techniques like second harmonic or sum-frequency generation, the laser irradiance can be low enough to avoid any disturbance of the fragile interface during the formation of the silica film. In-situ Raman spectroscopy experiments have also shown that Si-O-Si bands are observed after thermal treatment of the silica deposits. This experimental set-up could be then used to follow *in-situ* the functionalization of silica deposit via the co-condensation of silanes and organosilanes.

Acknowledgements

LP is grateful to Ecole Doctorale SESAMES (ED 412, Université de Lorraine) for his PhD grant The authors are thankful to the Région Lorraine for financial support. Tyndall National Institute (Cork, Ireland) is acknowledged for the provision of the silicon membranes. Dr Jérôme Grausem is thanked for technical support.

References

1. Z. Samec, *Pure Appl. Chem.*, 2004, **76**, 2147–2180.
2. H. A. Santos, V. García-Morales, and C. M. Pereira, *ChemPhysChem*, 2010, **11**, 28–41.
3. D. W. M. Arrigan, *Anal. Lett.*, 2008, **41**, 3233–3252.

4. D. W. M. Arrigan, G. Herzog, M. D. Scanlon, and J. Strutwolf, in *Electroanalytical Chemistry, Vol. 25*, eds. A. J. Bard and C. G. Zoski, CRC Press, Boca Raton, 2013, pp. 105–178.

5. A. Berduque, A. Sherburn, M. Ghita, R. A. W. Dryfe, and D. W. M. Arrigan, *Anal. Chem.*, 2005, **77**, 7310–7318.

6. J. B. Edel, A. A. Kornyshev, and M. Urbakh, *ACS Nano*, 2013, **7**, 9526–32.

7. M. Platt, R. A. W. Dryfe, and E. P. L. Roberts, *Electrochim. Acta*, 2004, **49**, 3937–3945.

8. C. Johans, R. Lahtinen, K. Kontturi, and D. J. Schiffrin, *J. Electroanal. Chem.*, 2000, **488**, 99–109.

9. B. Su, J.-P. Abid, D. J. Fermín, H. H. Girault, H. Hoffmannová, P. Krtil, and Z. Samec, *J. Am. Chem. Soc.*, 2004, **126**, 915–919.

10. A. Uehara, T. Hashimoto, and R. a. W. W. Dryfe, *Electrochim. Acta*, 2014, **118**, 26–32.

11. R. Knake, A. W. Fahmi, S. A. M. Tofail, J. Clohessy, M. Mihov, and V. J. Cunnane, *Langmuir*, 2005, **21**, 1001–8.

12. V. Mareček and H. Jänchenová, *J. Electroanal. Chem.*, 2003, **558**, 119–123.

13. L. Poltorak, G. Herzog, and A. Walcarius, *Electrochem. Commun.*, 2013, **37**, 76–79.

14. L. Poltorak, G. Herzog, and A. Walcarius, *Langmuir*, 2014, **30**, 11453–11463.

15. A. Walcarius, *Chem. Soc. Rev.*, 2013, **42**, 4098–140.

16. A. Walcarius, E. Sibottier, M. Etienne, and J. Ghanbaja, *Nat. Mater.*, 2007, **6**, 602–608.

17. A. Walcarius, *Anal. Bioanal. Chem.*, 2010, **396**, 261–72.

18. D. J. Fermin, in *Diffraction and Spectroscopic Methods in Electrochemistry*, eds. R. C. Alkire, D. M. Kolb, J. Lipkowski, and P. N. Ross, Wiley- VCH, Weinheim, 2006, pp. 127–162.

19. Z. Ding, R. G. Wellington, P. Brevet, and H. H. Girault, *J. Electroanal. Chem.*, 1997, **420**, 35–41.

20. D. Izquierdo, A. Martinez, A. Heras, J. Lopez-Palacios, V. Ruiz, R. A. W. Dryfe, and A. Colina, *Anal. Chem.*, 2012, **84**, 5723–30.

21. Y. Gründer, J. F. W. Mosselmans, S. L. M. Schroeder, and R. A. W. Dryfe, *J. Phys. Chem. C*, 2013, **117**, 5765–5773.

22. T. Kakiuchi, K. Ono, Y. Takasu, J. Bourson, and B. Valeur, *Anal. Chem.*, 1998, **70**, 4152–6.

23. T. Kakiuchi and Y. Takasu, *J. Electroanal. Chem.*, 1994, **365**, 293–297.

24. H. Nagatani, R. A. Iglesias, D. J. Fermin, P.-F. Brevet, and H. H. Girault, *J. Phys. Chem. B*, 2000, **104**, 6869–6876.

25. H. Wang, E. Borguet, and K. B. Eisenthal, *J. Phys. Chem. B*, 1998, **5647**, 4927–4932.

26. C. Amatore, F. Bonhomme, J.-L. Bruneel, L. Servant, and L. Thouin, *J. Electroanal. Chem.*, 2000, **484**, 1–17.

27. S. Szunerits, P. Garrigue, J.-L. Bruneel, L. Servant, and N. Sojic, *Electroanalysis*, 2003, **15**, 548–555.

28. H. G. M. Edwards, M. A. Hughes, and D. N. Smith, *Vib. Spectrosc.*, 1996, **10**, 281–289.

29. S. Yamamoto, K. Fujiwara, and H. Watarai, *Anal. Sci.*, 2004, **20**, 1347–1352.

30. S. Yamamoto and H. Watarai, *Langmuir*, 2006, **22**, 6562–9.

31. B. Das, U. Maitra, K. Biswas, N. Varghese, and C. N. R. Rao, *Chem. Phys. Lett.*, 2009, **477**, 160–163.

32. S. Guo, S. Dong, and E. Wang, *Cryst. Growth Des.*, 2009, **9**, 372–377.

33. S. G. Booth, D. P. Cowcher, R. Goodacre, and R. A. W. Dryfe, *Chem. Commun.*, 2014, 4482–4484.

34. M. De Serio, H. Mohapatra, R. Zenobi, and V. Deckert, *Chem. Phys. Lett.*, 2006, **417**, 452–456.

35. J. M. Perera and G. W. Stevens, *Anal. Bioanal. Chem.*, 2009, **395**, 1019–32.

36. I. Kaminska, M. Jonsson-Niedziolka, A. Kaminska, M. Pisarek, R. Hołyst, M. Opallo, and J. Niedziolka-Jonsson, *J. Phys. Chem. C*, 2012, **116**, 22476–22485.

37. R. Zazpe, C. Hibert, Y. H. Lanyon, J. O'Brien, and D. W. M. Arrigan, *Lab Chip*, 2007, **7**, 1732–1737.

38. D. Lin-Vien, N. B. Colthup, W. G. Fateley, and J. G. Grasselli, *The Handbook of Infrared and Raman Characteristic Frequencies of Organic Molecules*, Academic Press, London, 1991.

39. M. Kato, I. Abe, and Y. Taniguchi, *J. Chem. Phys.*, 1999, **110**, 11982.

40. J. R. Durig, T. S. Little, T. K. Gounev, J. K. Gardner Jr, and J. F. Sullivan, *J. Molec. Struct.*, 1996, **375**, 83–94.

41. F. O. Laforge, J. Carpino, S. A. Rotenberg, and M. V Mirkin, *Proc. Natl. Acad. Sci. U. S. A.*, 2007, **104**, 11895–900.

42. S. E. C. Dale and P. R. Unwin, *Electrochem. Commun.*, 2008, **10**, 723–726.

43. T. Wangchareansak, M. A. Keniry, G. Liu, and V. S. J. Craig, *Langmuir*, 2014, **30**, 6704–12.

44. Y. Guillemin, J. Ghanbaja, E. Aubert, M. Etienne, and A. Walcarius, *Chem. Mater.*, 2014, **26**, 1848–1858.

45. A.-R. Badiei, S. Cantournet, M. Morin, and L. Bonneviot, *Langmuir*, 1998, **14**, 7087–7090.

46. K. Biswas and C. N. R. Rao, *J. Colloid Interface Sci.*, 2009, **333**, 404–10.

47. B. Adeniran and R. Mokaya, *Chem. Mater.*, 2012, **24**, 4450–4458.

48. S. Wonorahardjo, G. E. Ball, J. Hook, and G. Moran, *J. Non-Cryst. Solids*, 2000, **271**, 137–146.

49. F. Marlow, M. D. McGehee, D. Zhao, B. F. Chmelka, and G. D. Stucky, *Adv. Mater.*, 1999, **11**, 632–636.